Concerted but Noncooperative Activation of Nucleotide and Actuator Domains of the Ca-ATPase upon Calcium Binding[†]

Baowei Chen,[‡] James E. Mahaney,[§] M. Uljana Mayer,[‡] Diana J. Bigelow,[‡] and Thomas C. Squier*[,‡]

Pacific Northwest National Laboratory, P.O. Box 999, Richland, Washington 99352, and Virginia College of Osteopathic Medicine, Blacksburg, Virginia 24060

Received July 30, 2008; Revised Manuscript Received September 4, 2008

ABSTRACT: Calcium-dependent domain movements of the actuator (A) and nucleotide (N) domains of the SERCA2a isoform of the Ca-ATPase were assessed using constructs containing engineered tetracysteine binding motifs, which were expressed in insect High-Five cells and subsequently labeled with the biarsenical fluorophore 4′,5′-bis(1,3,2-dithioarsolan-2-yl)fluorescein (FlAsH-EDT_2). Maximum catalytic function is retained in microsomes isolated from High-Five cells and labeled with FlAsH-EDT_2. Distance measurements using the nucleotide analog 2′,3′-*O*-(2,4,6-trinitrophenyl) adenosine 5′-triphosphate (TNP-ATP), which acts as a fluorescence resonance energy transfer (FRET) acceptor from FlAsH, identify a 2.4 Å increase in the spatial separation between the N- and A-domains induced by high-affinity calcium binding; this structural change is comparable to that observed in crystal structures. No significant distance changes occur across the N-domain between FlAsH and TNP-ATP, indicating that calcium activation induces rigid body domain movements rather than intradomain conformational changes. Calcium-dependent decreases in the fluorescence of FlAsH bound, respectively, to either the N- or A-domains indicate coordinated and noncooperative domain movements, where both A- and N-domains display virtually identical calcium dependencies (i.e., $K_d = 4.8 \pm 0.4$ μM). We suggest that occupancy of a single high-affinity calcium binding site induces the rearrangement of the A- and N-domains of the Ca-ATPase to form an intermediate state, which facilitates phosphoenzyme formation from ATP upon occupancy of the second high-affinity calcium site.

P-type ATPases form a family of primary ion transporters that utilize ATP to actively transport a wide range of different ions against a concentration gradient, acting to control many different fundamental biological processes ranging from muscle contraction and nerve conduction to the extrusion of toxic metals from cells (*1*). Important insights regarding ion transport mechanisms for this family of P-type ATPases have been obtained from the wealth of structural information available for the sarco/endoplasmic reticulum Ca-ATPase (SERCA),[1] including the 25 atomic resolution structures crystallized in nine different enzyme intermediate states (*2*−*5*). These crystal structures confirm earlier spectroscopic measurements that established that ATP binds within a nucleotide binding domain that is spatially distant (i.e., >50 Å) from calcium ion binding sites located near the bilayer center (*6*−*8*) and that large amplitude domain motions couple ATP hydrolysis to ion transport (*2, 5, 9*−*14*). Movements of three cytosolic regions, that is, the nucleotide binding (N), phosphorylation (P), and actuator (A) domains (Figure 1), are modulated by large rearrangements of transmembrane helices in response to calcium occupancy of high affinity sites. These changes act to reposition the N-domain relative to the P-domain, thus promoting the transfer of the γ-phosphoryl group of ATP to Asp^{351}, which forms a phosphoenzyme intermediate within the P-domain (*5*).

Solution structures using probes bound to the N- and P-domains have been measured and are consistent with high-resolution X-ray structures (*9, 10*). Coordinated motions of the actuator (A) domain are proposed to facilitate the association between the N- and P-domains necessary for phosphoenzyme formation and calcium occlusion (*5*). However, it remains unclear whether the large amplitude motions of the A-domain apparent in high-resolution crystal structures accurately reflect average structures in solution (*15, 16*). Furthermore, as crystal structures depict the fully activated

[†] This work was supported by the National Institutes of Health (Grant HL64031) and Genomics:GTL program (Grant 45701) within the Office of Biological and Environmental Research at the U.S. Department of Energy. Pacific Northwest National Laboratory is operated for the Department of Energy by Battelle Memorial Institute under Contract DE-AC05-76RLO 1830.

* To whom correspondence should be addressed. Mailing address: Pacific Northwest National Laboratory, P.O. Box 999, Mail Stop P7-53; Richland, WA 99352. E-mail: thomas.squier@pnl.gov. Tel: 509-376-2218. Fax: 509-372-1632.

[‡] Pacific Northwest National Laboratory.

[§] Virginia College of Osteopathic Medicine.

[1] Abbreviations: A-domain, actuator domain; β-ME, β-mercaptoethanol; DMPS, 2,3-dimercapto-1-propanesulfonic acid; EDT, 1,2-ethanedithiol; EDTA, ethylenediaminetetraacetic acid; EGTA, ethylene glycol bis(β-aminoethylether)-*N*,*N*,*N*′,*N*′-tetraacetic acid; FlAsH-EDT_2, 4′,5′-bis(1,3,2-dithioarsolan-2-yl)fluorescein; FRET, fluorescence resonance energy transfer; MOPS, 3-(*N*-morpholino)propanesulfonic acid; N-domain, nucleotide binding domain; P-domain, phosphorylation domain; SERCA, sarco/endoplasmic reticulum Ca-ATPase; SDS−PAGE, sodium dodecyl sulfate−polyacrylamide gel electrophoresis; TCEP, tris(carboxyethyl)phosphine; TM, transmembrane; TNP-ATP, 2′,3′-*O*-(2,4,6-trinitrophenyl) adenosine 5′-triphosphate.

10.1021/bi8014289 CCC: $40.75
Published on Web 10/29/2008

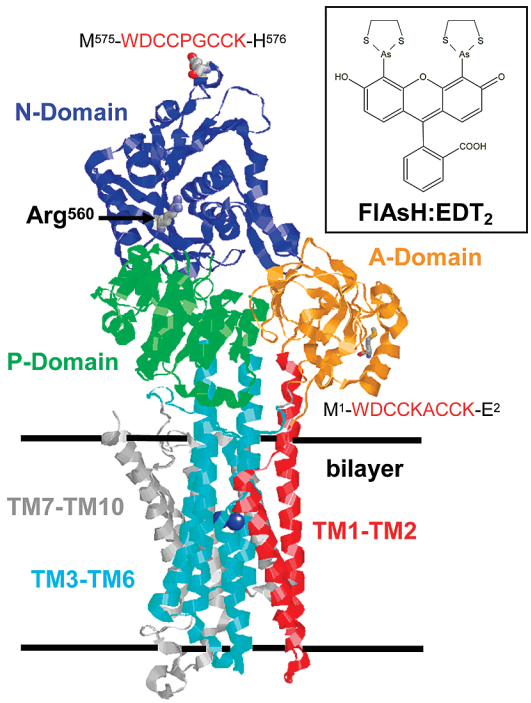

FIGURE 1: Locations of engineered labeling motifs within A- and N-domains of the Ca-ATPase. The headpiece corresponding to the A-domain (residues 1−43 and 124−235; orange), N-domain (residues 360−600; dark blue), and P-domain (residues 330−359 and 601−739; green) consists of three discrete structural elements relative to transmembrane helices TM1−TM2 (residues 44−123; red), TM3−TM6 (residues 239−329 and 740−821; cyan), and TM7−TM10 (residues 831−994; gray) (1su4.pdb), where domain boundaries are as previously described (*7*). Positions of FlAsH labeling are shown (CPK shaded side chains), and represent the insertion point corresponding to different constructs with either M^1-WDCCKACCK-E^2 on the A-domain or M^{575}-WDCCPGCCK-H^{576} on the N-domain. Arg^{560} represents a reference point located in the nucleotide binding pocket and acts to stabilize the α-phosphate of bound ATP (*13*). Inset shows structure of 4′,5′-bis(1,3,2-dithioarsolan-2-yl)fluorescein (FlAsH-EDT_2).

enzyme bound to two calcium ions, it is uncertain how conformational rearrangements of cytoplasmic domains contribute to intermediate enzyme states associated specifically with cooperative binding of the second calcium ion (*5, 17*).

To examine how calcium binding promotes the activation of the Ca-ATPase through changes in average domain conformation, and the relevance of reported crystal structures to the average conformation of the enzyme in solution, we have used molecular probes to label sites engineered into separate constructs of SERCA2a on the nucleotide and actuator domains of the Ca-ATPase. These measurements utilize the biarsenical fluorescent probe 4′,5′-bis(1,3,2-dithioarsolan-2-yl)fluorescein (FlAsH), which binds through a unique tetracoordinate linkage to four introduced cysteines engineered in a tagging sequence loop in the A-domain (i.e., M^1-WDCCKACCK-E^2) or the N-domain (i.e., M^{575}-WDCCPGCCK-H^{576}). These constructs permit the selective labeling of sites in the Ca-ATPase expressed in microsomes (*18*) (Figure 1). The ability to selectively label the engineered tagging sequence using biarsenical probes permits structural changes to be measured in isolated microscomes and avoids the requirement for the engineering of mutant proteins to contain single reactive thiols that have to be labeled following their purification and prior to their functional reconstitution (*19*−*21*).

Using the nucleotide analog TNP-ATP as a fluorescence resonance energy transfer (FRET) acceptor, we find that the spatial separation between the biarsenical probe FlAsH bound to either the A- or N-domains and TNP-ATP is in excellent agreement with prior crystal structures of the Ca-ATPase (*7, 8, 22*). Further, we detect coordinated and noncooperative changes in the fluorescence signals from FlAsH bound to the A- and N-domains of the Ca-ATPase upon calcium activation, which indicate that conformational rearrangements associated with enzyme activation involve linked domain movements through direct coupling to occupancy of a single high-affinity calcium binding site.

EXPERIMENTAL PROCEDURES

Materials. 4′,5′-Bis(1,3,2-dithioarsolan-2-yl)fluorescein (FLAsH-EDT_2) was synthesized as previously described (*23, 24*). *N*-(2-Hydroxyethyl)piperazine-*N*′-(2-ethanesulfonic acid) (HEPES), tris(carboxyethyl)phosphine (TCEP), β-mercaptoethanol (β-ME), and 1,2-ethanedithiol (EDT) were obtained from Sigma-Aldrich (Milwaukee, WI). All other chemicals were the purest grade commercially available.

DNA Constructs and Vectors. The rat cardiac muscle sarcoplasmic reticulum Ca-ATPase (SERCA2a) cDNA used for these studies was the kind gift of Dr. Jonathan Lytton, University of Calgary. This SERCA2a cDNA was subcloned into the pMT2 vector at the *Eco*RI sites, but the cDNA also contained a single *Eco*RI restriction site (1443-GAATTC-1448) within the open reading frame. To remove the internal *Eco*RI restriction site, a silent mutation (1443-GAGTTC-1448) was made using the QuikChange II XL site-directed mutagenesis system and XL10-Gold ultracompetent cells (Agilent Technologies (Stratagene), La Jolla, CA). The correct mutation was confirmed by DNA sequencing and by *Eco*RI restriction analysis of the mutated SERCA2a pMT2 construct. Next, the SERCA2a cDNA was excised from the pMT2 vector using *Eco*RI restriction digestion and subcloned into the *Eco*RI site in the pVL1392 baculovirus transfer vector (BD Biosciences Pharmingen Inc., San Diego, CA). The correct orientation of the SERCA2a cDNA was confirmed by DNA sequencing at the junction of the pVL1392 and SERCA2a cDNA and by restriction analysis, taking advantage of the single *Bgl*II restriction site in the pVL1392 multicloning site and the single *Bgl*II restriction site in the SERCA2a cDNA open reading frame. At that time, the decision was made to utilize the Bac-to-Bac baculovirus expression system (Invitrogen Inc., Carlsbad, CA). Therefore the rat SERCA2a cDNA was excised from pVL1392 using the restriction enzymes *Not*I and *Xba*I, then subcloned into the corresponding sites in the pFastBac1 baculovirus transfer vector multicloning site (Invitrogen). All subsequent mutagenesis work was carried out using this construct.

SERCA2a Mutagenesis. Two tetracysteine motif SERCA2a constructs were made. The first contained the amino acid sequence Trp-Asp-Cys-Cys-Lys-Ala-Cys-Cys-Lys inserted between Met^1 and Glu^2 in the A-domain of wild-type SERCA2a. The second construct contained the amino acid sequence Trp-Asp-Cys-Cys-Pro-Gly-Cys-Cys-Lys inserted in the N-domain between Met^{575} and His^{576} in the wild-type sequence. The insertion mutants were made using the

QuikChange XL site-directed mutagensis system and XL10-Gold ultracompetent cells (Stratagene). The presence of the insert was confirmed by cDNA sequencing.

Recombinant Baculovirus Preparation. All baculovirus preparation work was carried out using serum-free Sf-21 cells from PharMingen. Recombinant baculoviruses containing either the wild-type SERCA2a cDNA or the tetracysteine SERCA2a construct cDNAs were prepared using the Bac-to-Bac baculovirus expression system (Invitrogen). The presence of the given cDNA in the recombinant bacmid was verified by PCR analysis according to the manufacturer's instructions, except that M13 forward and M13 reverse PCR primers from Integrated DNA Technologies were used in place of the corresponding primers recommended by Invitrogen. Passage 1 viral stocks for each construct were generated according to the manufacturer's instructions. The viral stock was plaque-purified, and the resultant virus solution was amplified twice to produce a high-titer stock. Viral titer in the stock solutions was determined using the BacPAK baculovirus rapid titer kit (Clontech Inc., Mountain View, CO). Baculovirus stocks typically had a titer of 1×10^8 pfu/mL or greater and were stored at 4 °C in the dark.

Protein Expression and Characterization. SERCA2a (wild-type and mutant) was expressed in High-Five insect cells (Invitrogen) as reported elsewhere (*25*). Microsomes were harvested 48 h after baculovirus infection and stored in small aliquots at −80 °C. Protein concentrations were measured (*26*) using bovine serum albumin (Sigma) as a standard. The amount of SERCA2a in the microsomes was quantified by gel electrophoresis and immunoblotting to correspond to about 1.5% of expressed protein, using methods described previously (*25*). For the immunoblotting, the anti-SERCA2a monoclonal antibody 2A7-A1 (Affinity Bioreagents, Golden, CO) was the primary antibody used, and protein A conjugated with horseradish peroxidase (BioRad Inc., Hercules, CA) was used as the secondary antibody. Immunoblots were developed colorimetrically using the horseradish peroxidase assay (BioRad) and analyzed by densitometry. This permitted the measurement of expression levels of the two SERCA2a tetracysteine motif mutant constructs relative to wild-type enzyme.

SERCA2a Activity Assays. Ca^{2+} concentration-dependent rates of ATP hydrolysis were measured using High-Five insect cell microsomes (0.05 mg/mL) in 50 mM MOPS (pH 7.0), 3.0 mM $MgCl_2$, 100 mM KCl, 1.0 mM EGTA, and variable amounts of $CaCl_2$ to give the desired ionized Ca^{2+} concentration, as previously determined (*25*), where the formation of inorganic phosphate was measured using a colorimetric malachite green−ammonium molybdate assay (ATPase activity), as previously described (*25*). To initiate the ATPase reaction, 5 mM MgATP was added to the incubation tube at 37 °C, and inorganic phosphate liberation was measured as a function of time. SERCA2a samples were pretreated with 20 μg of the calcium ionophore A23187 per milligram of total protein to prevent Ca^{2+} build-up within the microsome during the assay. Calcium-dependent activity curves were fit using the Hill equation fitting function.

Labeling with FLAsH-EDT$_2$. Following incubation of microsomes (8 mg/mL) in 150 mM MOPS (pH 7.0) with 10 mM β-ME and 10 mM TCEP for 1 h at 25 °C, the tetracysteine motif engineered into either the A- or N-domains of the Ca-ATPase were reacted with FlAsH-EDT$_2$ (15 μM) for 30 min at 25 °C. Samples were diluted 3-fold to stop the reaction into 150 mM MOPS/TRIS (pH 7.0) and 50 μM DMPS, and unbound probe was separated from microsomes by two successive centrifugation steps (100 000 × *g* for 45 min). The resulting pellet was resuspended in 150 mM MOPS/TRIS (pH 7.0). Labeled proteins were imaged using a Kodak IS2000MM imager (Rochester, NY), using interference filters centered at 465 nm for excitation and 535 nm for detection.

Fluorescence Measurements. Fluorescence measurements used a Fluoro Max-2 fluorometer (SPEX, Edison, NJ), using exitation and emission slits of 5 nm. In all cases, the sample temperature was 25 °C. Changes in the solvent accessibility of FlAsH were assessed through collisional quenching, where variable amounts of acrylamide were added to FlAsH-labeled SERCA expressed in microsomes (50 μg/mL). Data were analyzed as F_0/F as a function of the titrated acrylamide concentration and according to the Stern−Volmer equation:

$$F_0/F = 1 + K_{sv}[Q] \quad (1)$$

where F_0 and F are the respective fluorescence intensities in the absence and presence of added acrylamide [Q]. K_{sv} is the Stern−Volmer quenching constant (*27*).

RESULTS

Expression and Activity of the Ca-ATPase. Wild-type rat SERCA2a and mutants that contain tetracysteine tagging sequences inserted into nonconserved regions in the N- or A-domains were expressed in High-Five insect cells. Quantitative immunoblots and a consideration of fluorescent labeling (see below) indicate that the Ca-ATPase represents about 1.5% of the expressed protein in these preparations and that there is very little endogenous SERCA in these insect microsomes. Consistent with their small size, the introduction of tetracysteine binding motifs engineered in the N-domain (i.e., M^{575}-WDCCPGCCK-H^{576}) or the A-domain (i.e., M^1-WDCCKACCK-E^2) has a minimal effect on either the abundance of SERCA2a in isolated microsomes or the migration of SERCA2a on SDS−PAGE, indicating that these tagging sequences do not dramatically affect the overall enzyme conformation to induce, for example, irreversible protein associations. Further, the expressed Ca-ATPase retains full activity irrespective of the introduction of tetracysteine tagging sequences, where maximal rates of ATP hydrolysis (i.e., 30 μmol P_i/(mg min)) are comparable to SERCA2a activity observed in microsomes isolated from hearts upon correcting for relative differences in SERCA2a abundance (Figure 2) (*28*).

Targeted Labeling of SERCA Using Biarsenical Probes. Microsomes were labeled using the biarsenical probe FlAsH-EDT$_2$ (Figure 1), where the bound ethanedithiol (EDT) is displaced upon association of each arsenic with a pair of vicinal cysteines in the tagging sequence. Prior measurements have established the specificity of FlAsH-EDT$_2$ for the labeling of tagged proteins in complex environments. Subsequently FlAsH was used for functional imaging of protein conformational changes, which is facilitated by the small size and tetracoordinate linkage of the probe (*18, 23, 24, 29*−*33*).

SERCA2a constructs with engineered tagging sequences in either the A- or N-domains are preferentially labeled by incubation with FlAsH-EDT$_2$ for 30 min, each arsenic

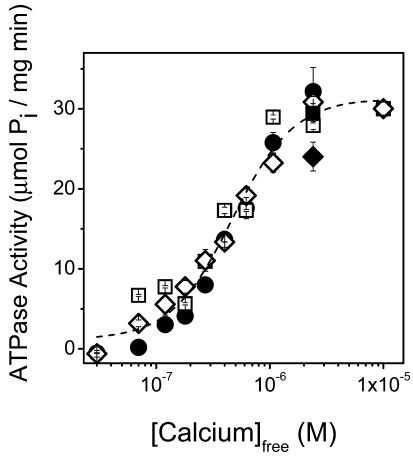

FIGURE 2: Catalytic function of wild-type and engineered constructs of the Ca-ATPase. Rates of ATP hydrolysis were measured for the Ca-ATPase in High-Five insect cell microsomes (50 μg/mL) expressing wild-type rat SERCA2a (●) or engineered constructs with tetracysteine insertion sequences in the A-domain (◇, ◆) or N-domain (□, ■) of the Ca-ATPase prior to (◇, □) or following (◆, ■) incubation with FlAsH-EDT_2. ATPase activity was measured at 37 °C in 50 mM MOPS (pH 7.0), 0.1 M KCl, 3 mM $MgCl_2$, 1 mM EGTA, and sufficient $CaCl_2$ to yield the desired ionized calcium concentration, as previously determined (*25*). The reaction was initiated upon addition of 5 mM MgATP. The dashed line represents the fit to the Hill equation, where $n = 1.6 \pm 0.2$ and $K_d = 0.47 \pm 0.05$ μM free calcium. Maximal ATPase activities were normalized to the abundance of SERCA2a, where quantitative immunoblotting indicates that the Ca-ATPase represents on average about 1.5% of the total protein in isolated microsomes.

chelating a pair of vicinal cysteine ligands (Figure 3A). In the absence of competing 2,3-dimercapto-1-propanesulfonic acid (DMPS), labeling is not absolutely specific, as evidenced by the multiple labeled proteins in addition to the Ca-ATPase visible under UV light. Nonspecific labeling is particularly pronounced in control experiments that involve expression of wild-type SERCA2a with no engineered tagging sequence. However, the tetracysteine tagged SERCA2a constructs compete more effectively for added FlAsH-EDT_2 than nonspecific sites.

Considerable improvements in labeling specificity are possible if DMPS is added following labeling with FlAsH-EDT_2 to displace FlAsH bound to lower affinity nonspecific sites. Addition of 50 μM DMPS is sufficient to effectively eliminate nonspecific binding at all sites that do not contain the tetracysteine tagging sequence (Figure 3A). In this respect, it is notable that wild-type SERCA2a, which lacks the tetracysteine tagging sequence, is not labeled under these conditions, demonstrating that there is minimal nonspecific labeling of the Ca-ATPase itself (see lane 1 in Figure 3A). Some unbound (i.e., free) FlAsH-EDT_2 is apparent near the dye front under these conditions that can be removed by centrifugation of labeled microsomes (Figure 3B). Thus, we demonstrate the facile ability to selectively label the tagged Ca-ATPase, with background signals associated with nonspecific labeling by FlAsH accounting for less than 9% of the total fluorescence signal (Figure 3C).

Coordinated and Noncooperative N- and A-Domain Motions upon Calcium Binding. An ability to selectively label individual sites on the A- and N-domains of SERCA in native microsomes provides a means, for the first time, to simultaneously assess movements between these key domain elements upon calcium activation of the Ca-ATPase. Calcium-dependent conformational changes were assessed from a consideration of both (i) solvent accessibilities to the collisional quencher acrylamide and (ii) fluorescence intensity changes for FlAsH bound to either the A- or N-domains of the Ca-ATPase. Prior to calcium activation, the solvent accessibilities of FlAsH bound to either the A- or N-domains of the Ca-ATPase are very similar (Figure 4). Upon calcium activation, there is a large increase in the solvent exposure of FlAsH bound to the A-domain as evidenced by the increased slope. Increases in solvent exposure at this labeling site are consistent with high-resolution structures, where calcium activation results in a large reorientation of the A-domain that repositions the tagging sequence away from the interdomain interface with the N-domain (i.e., 1iwo.pdb vs 1su4.pdb) (*34*). These large movements of the A-domain are proposed to allow the N- and P-domains to move into closer proximity to facilitate phosphoenzyme formation (*3, 22*). In comparison, there are no significant changes in the solvent accessibility of FlAsH bound to the N-domain upon calcium activation, as is expected from the relatively modest calcium-dependent changes in the orientation and structure of the N-domain in available high-resolution structures. Observed changes in the solvent accessibilities of FlAsH bound to the A- or N-domains upon calcium activation are further reflected by the magnitude of the fluorescence intensity, as the fluorescence intensity of FlAsH bound to either the A- or N-domains, respectively, decreases by 23% and 9% upon calcium activation of the Ca-ATPase (Figure 5A,B).

Using changes in the fluorescence intensity of FlAsH bound to either the A- or N-domains to monitor their calcium-dependent activation, we observe that both signals increase with calcium concentrations but to different extents. However, essentially identical calcium dependencies are observed, which suggests coordinated movements following calcium binding (Figure 5C). Upon fitting both data sets, we find that the macroscopic dissociation constant (K_d) obtained from fitting the data to the Hill equation is 0.48 ± 0.04 μM, which is essentially identical to that associated with the calcium-dependent activation of ATP hydrolysis (Figure 2). However, in contrast to observed calcium-dependent increases in rates of ATP hydrolysis ($n_H = 1.6 \pm 0.2$) (Figure 2), we observe that calcium-dependent transitions involving both the A- and N-domains are noncooperative with a Hill coefficient (n_H) of 0.93 ± 0.07 (Figure 5C). These latter results suggest that occupancy of a single high-affinity calcium binding site is sufficient to mediate the large conformational changes apparent in the crystal structure.

Changes in Spatial Arrangement of A- and N-Domains upon Calcium Activation. From available high-resolution crystal structures, high levels of ATP in the cell are suggested to modulate the structure of the Ca-ATPase, acting to maintain a compact headpiece organization (*22*). Movements of the A-domain are proposed to play a central role in mediating concerted movements of transmembrane helices upon calcium binding that promote phosphoenzyme formation from ATP (*3*). In the case of the A-domain, sensitivities of proteinase K cleavage sites Leu^{119} and Thr^{242} in stalk regions connecting the A-domain to the transmembrane helices have provided a means to assess ligand-dependent structural changes in solution. These measurements confirm that calcium binding induces an A-domain reorganization that acts to expose Thr^{242} for proteolytic cleavage (compare

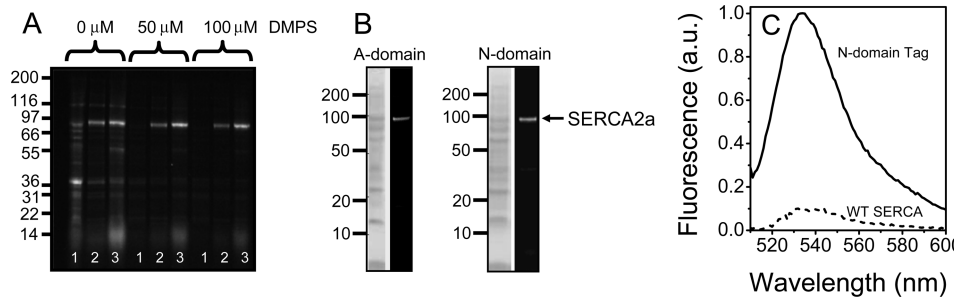

FIGURE 3: Selective Labeling of the Ca-ATPase Expressed in High-Five Microsomes. (A) fluorescence signals from FlAsH-labeled proteins following SDS−PAGE separation of microsomal proteins (40 μg) expressing wild-type SERCA2a (lane 1) or engineered constructs containing insertion sequences in the A-domain (lane 2) or N-domain (lane 3) assayed immediately after incubation with FlAsH-EDT$_2$ (5 μM) for 10 min at 25 °C in the presence of 5 mM β-ME and 5 mM TCEP and the indicated amount of 2,3-dimercapto-1-propanesulfonic acid (DMPS) to reduce nonspecific binding (*18*); (B) Coomassie blue protein stain (left lanes) or fluorescence (right lanes) imaging following FlAsH labeling, incubation in DMPS (50 μM), and SDS−PAGE separation of High-Five insect cell microsomes (10 μg) expressing engineered SERCA2a, where the insertion sequence is within the A- (WDCCKACCK) or N-domain (WDCCPGCCK) of the Ca-ATPase; (C) fluorescence emission spectra of High-Five insect microsomes (0.1 mg/mL) expressing either wild-type SERCA (dashed line) or the engineered N-domain tag (solid line) following incubation with FlAsH-EDT$_2$ (10 μM), where λ_{ex} = 500 nm. The fluorescence emission spectrum of FlAsH-labeled vesicles expressing the A-domain tag were virtually identical to that shown using the N-domain tag.

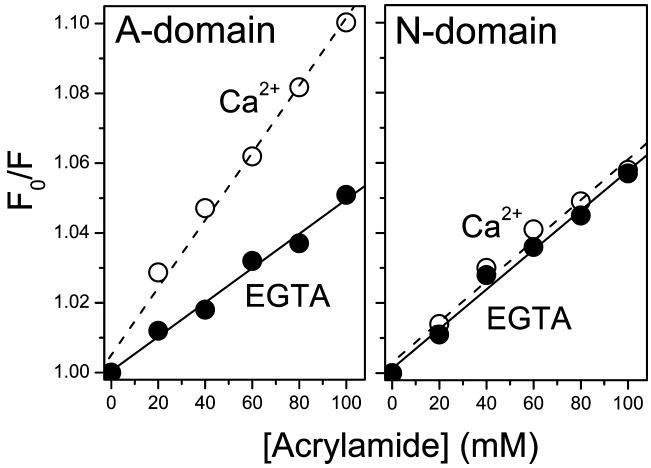

FIGURE 4: Solvent accessibilities of FlAsH bound to A-domain or N-domain of the Ca-ATPase. Stern−Volmer quenching was measured as decreases in the fluorescence intensity (F) relative to the initial value (F_0) for FlAsH-labeled microsomes expressing SERCA2a (50 μg/mL) in 150 mM MOPS (pH 7.0) and 5 mM $MgCl_2$ in the presence of either 2 mM EGTA (●) or 0.2 mM $CaCl_2$ (○) at 25 °C. Slopes of the lines (i.e., the Stern−Volmer quenching constant, K_{sv}) for the A-domain are 0.49 ± 0.03 M^{-1} (EGTA) and 0.96 ± 0.05 M^{-1} (Ca^{2+}); for the N-domain K_{sv} = 0.56 ± 0.03 M^{-1} (EGTA) or 0.58 ± 0.04 M^{-1} (Ca^{2+}). λ_{ex} = 500 nm; λ_{em} = 530 nm.

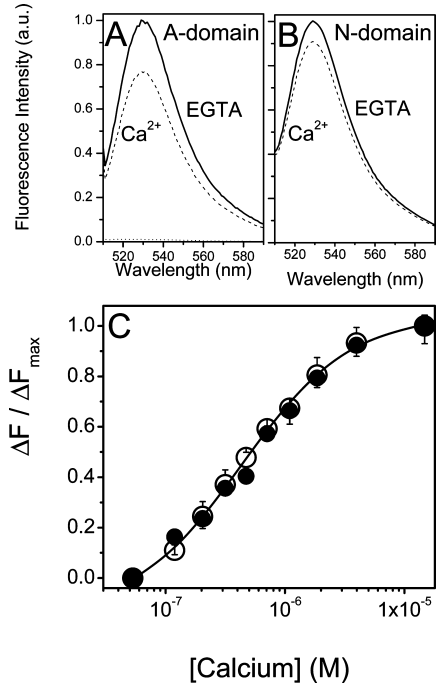

FIGURE 5: Calcium-dependent conformational sensitivity of A-domain (panel A; ○ in panel C) or N-domain (panel B; ● in panel C) constructs of FlAsH-labeled SERCA2a (50 μg/mL) in 150 mM MOPS/TRIS (pH 7.0), 5 mM $MgCl_2$, 0.5 mM EGTA, and sufficient calcium to yield the indicated ionized (free) calcium concentration. Values represent averages and standard errors of the mean from three independent measurements, where λ_{ex} = 500 nm and λ_{em} = 530 nm. Line in panel C represents nonlinear least-squares fit of both data sets to the Hill equation, where the macroscopic equilibrium constant K_d = 0.48 ± 0.04 μM and the Hill coefficient is 0.93 ± 0.07. Temperature was 25 °C.

1iwo.pdb with 1su4.pdb in Figure S1 in Supporting Information) (*12, 34, 35*). However, in the presence of bound nucleotide, there is no direct correspondence between the proteinase K cleavage sensitivities and surface accessibilities in high-resolution crystal structures (e.g., compare 2c88.pdb and 1t5s.pdb in Figure S2 in Supporting Information) (*12, 13*).

To ascertain whether the crystal structures reliably assess average structures of the Ca-ATPase in solution, we have measured the spatial relationship between FlAsH bound to the A- and N-domains of the Ca-ATPase and TNP-ATP bound to the N-domain. These distance measurements use FlAsH as a fluorescence resonance energy transfer (FRET) donor and TNP-ATP as a FRET acceptor, where prior measurements have demonstrated that TNP-ATP effectively substitutes for ATP in the nucleotide binding site but is not hydrolyzed under these experimental conditions (*36, 37*). The FlAsH labeling sites in the A- and N-domains permit us to assess calcium-dependent changes in both the interdomain spatial separation between A- and N-domains and possible intradomain distance changes across the N-domain.

Upon titration of TNP-ATP, we observe a progressive increase in energy transfer efficiency for FlAsH bound to either the A- or N-domains of the Ca-ATPase, which saturates in the presence of approximately 40 μM added TNP-ATP (Figure 6). Fitting these binding curves to the Hill equation, we find that the apparent dissociation constants are very similar to earlier measurements ($K_d \approx 10\ \mu$M) (*36, 38*). Prior to calcium binding (i.e., apo-form of the Ca-ATPase),

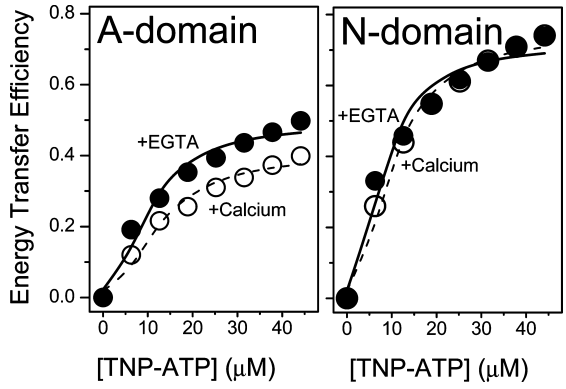

FIGURE 6: Calcium-dependent change in spatial separation between A- and N-domains. Fluorescence resonance energy transfer efficiency (E) was measured using FlAsH (donor) bound to either the A-domain or N-domain and TNP-ATP (acceptor), where $E = 1 - F_{da}/F_d$. F_{da} and F_d are the fluorescence intensity of FlAsH bound donor prior to and following saturation of the ATP binding site by the nucleotide analog TNP-ATP. Experiments were carried out using FlAsH-labeled microsomes expressing SERCA2a (12 μg protein/mL) in 150 mM MOPS/TRIS (pH 7.0) in the presence of either 0.2 mM $CaCl_2$ (○) or 2 mM EGTA (●). $\lambda_{ex} = 500$ nm, $\lambda_{em} = 530$ nm, and fluorescence intensities were corrected for the inner filter effect (*27*). Lines represent fits to the Hill equation, where for the A-domain $K_d = 13 \pm 2$ μM and $E_{max} = 0.39 \pm 0.03$ in the presence of calcium (○) and $K_d = 11 \pm 2$ μM and $E_{max} = 0.47 \pm 0.03$ in the presence of EGTA (●). For the N-domain, $K_d = 11 \pm 1$ μM and $E_{max} = 0.73 \pm 0.05$ in the presence of calcium (○) and $K_d = 9 \pm 1$ μM and $E_{max} = 0.69 \pm 0.05$ in the presence of EGTA (●).

the maximal energy transfer efficiencies between TNP-ATP and FlAsH bound to either the A- and N-domains are, respectively, 47% ± 3% and 69% ± 5%, which correspond to distances of 34.6 ± 0.7 Å and 30 ± 1 Å. These latter distances compare favorably with two reported high-resolution structures of the apo-form of the Ca-ATPase with the bound nucleotide AMPPCP (i.e., 2dqs.pdb and 2c88.pdb) (Table 1). In these two high-resolution crystal structures, the intermolecular distances between the protein backbone of the tagging insertion sequence in the A-domain and the 3′ position of the ribose insertion site for the TNP moiety bound to the N-domain are 34 and 36 Å. Intramolecular distances between the FlAsH-binding site in the N-domain and the bound nucleotide in the two available structures in the Protein Data Bank (http://www.rcsb.org/pdb) are 28 Å, which agrees favorably with our measured distance of 30 ± 1 Å.

Following calcium activation, there are no significant changes in the measured energy transfer efficiency between FlAsH bound to the N-domain and TNP-ATP (Figure 6B). This latter result indicates that there are no significant changes in the overall dimension of the N-domain upon calcium activation, in agreement with the high-resolution crystal structures (*5*). In comparison, we observe that there is a substantial decrease in the energy transfer efficiency between FlAsH bound to the A-domain and TNP-ATP, which decreases from 47% ± 3% for the apo-form of the enzyme to 39% ± 3% (Figure 6A). The 8% ± 4% decrease in FRET is indicative of a 2.4 ± 1.0 Å increase in the spatial separation between the A- and N-domains. This latter result is consistent with the reorientation of the A-domain apparent in the high-resolution crystal structure that acts to enhance the association between N- and P-domains necessary for nucleotide utilization (Figure 7). Together, these results indicate a central role for calcium binding in modulating interdomain interactions in both the absence and presence of bound nucleotide (Figures 5, 6, and 7) and argues against prior suggestions that "calcium binding has comparatively minor effects" in the presence of bound nucleotide (*11*).

DISCUSSION

We have expressed a fully functional SERCA2a isoform of the Ca-ATPase engineered to contain tetracysteine tagging sequences in either the A- or N-domains (Figure 2). Following isolation of microsomes, the encoded tagging sequence in the Ca-ATPase is labeled specifically using the small biarsenical probe FlAsH (Figures 1 and 4). We detect coordinated but noncooperative local structural changes of both the A- and N-domains upon calcium binding that suggest binding of a single calcium acts to reposition cytosolic domain elements (Figure 5C). There are only minimal changes in either the fluorescence intensity or solvent accessibility of FlAsH bound to the N-domain upon calcium activation, and no changes in the intradomain FRET efficiency between FlAsH bound to the N-domain and TNP-ATP. In contrast, large calcium-dependent changes in the solvent accessibilities and fluorescence intensities of FlAsH in the A-domain are observed (Figures 5 and 6), as well as a 2.4 Å increase in the interdomain distance between FlAsH and bound TNP-ATP upon calcium binding (Figure 6, Table 1). These measurements are consistent with the substantial reorientation of the A-domain observed in comparisons of crystal structures of the homologous SERCA1 in the absence (1iwo.pdb) and in the presence (1su4.pdb) of bound calcium (*4*) (Figure 7).

Prior measurements have demonstrated that the binding affinity of ATP to the Ca-ATPase is unaffected by calcium activation despite the fact that occupancy of calcium binding sites is necessary for the transfer of the γ-phosphate from bound ATP to Asp^{351} to form a phosphoenzyme intermediate (*12*). This observation is consistent with the millimolar ATP concentrations present in the cell and suggests that calcium binding acts to promote phosphoenzyme formation rather than nucleotide binding. Further, in view of the substantial amount of dynamic disorder associated with cytoplasmic domains of the Ca-ATPase (*2, 9, 10, 14, 39*), calcium binding may promote the adoption of an infrequent conformer required for phosphoenzyme formation. Insight into the molecular mechanism underlying calcium-dependent structural changes is possible from a consideration of the high-resolution structure, which reveals that the two high-affinity calcium binding sites are located near the center of the bilayer in the Ca-ATPase and share several common ligands (*5, 40*). However, it has remained uncertain how the association of either the first or second calcium may differentially modify the conformation of headpiece elements to affect phosphoenzyme formation from ATP (*5*). Our results, demonstrating a noncooperative movement of the A- and N-domains upon calcium activation, suggest that occupancy of each calcium site induces distinct sets of domain rearrangements. For example, binding of a single calcium may induce large-scale domain movements to create a more compact headpiece organization that enhances transfer of the γ-phosphoryl moiety from ATP upon repositioning Asp^{351} to facilitate its phosphorylation upon occupancy of the second calcium. In this respect, closely juxtaposed headpiece domains would have the potential to enhance transport efficiency, because

Table 1: Comparison between Solution and X-ray Structures[a]

	interdomain A-domain → N-domain distance (Å)			distance across N-domain (Å)		
	FRET	X-ray structure		FRET	X-ray structure	
enzyme state	(FlAsH → TNP-ATP)	(Met^1 → ribose)	(Met^1 → Arg^{560})	(FlAsH → TNP-ATP)	(Met^{576} → ribose)	(Met^{576} → Arg^{560})
E-ATP	34.6 ± 0.7			30 ± 1		
2dqs.pdb		34	35		28	28
2c88.pdb		36	38		28	30
2Ca-E-ATP	37.0 ± 0.7			29 ± 1		
1vfp.pdb		42	42		27	30
1t5s.pdb		42	39		28	29

[a] Solution measurements made using fluorescence resonance energy transfer (FRET) between FlAsH bound to tagging sequences on A- or N-domains and TNP-ATP in comparison to indicated high-resolution X-ray structures (*7, 8, 22*). Distances represent those between the amino group at the insertion position of the tag in SERCA1 structures and either the O_3' ribose position or the proximal NH_1 side chain of Arg^{560}, previously identified as a key interfacial residue that chelates bound ATP (*13, 47*) and within 4 Å from the O_3' ribose.

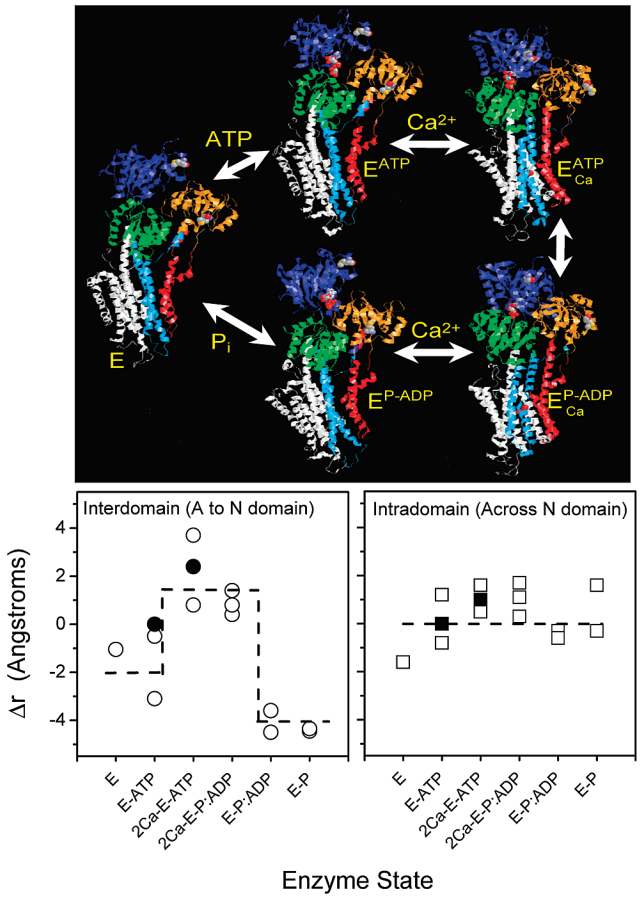

FIGURE 7: Headpiece domain reorientation and calcium activation. Depiction of selected crystal structures of the Ca-ATPase (top) using domain boundaries defined in the legend to Figure 1. Coordinates were used for the Ca-ATPase (i.e., E) stabilized in six different states, corresponding to (i) E, no calcium (1iwo.pdb; shown) (*35*), (ii) E−ATP (2dqs.pdb and 2c88.pdb (shown)) (*22*), (iii) 2Ca−E−ATP (1vfp.pdb and 1t5s.pdb (shown)) (*7, 8*), (iv) 2Ca−E−P:ADP (2zbd.pdb, 1t5t.pdb (shown), or 3ba6.pdb) (*3, 7, 48*), (v) E−P:ADP (3b9r.pdb or 1wpg.pdb (shown)) (*3, 48*), and (vi) E−P (3b9b.pdb and 1xp5.pdb) (*3, 49*). (bottom) Distance changes (Δr) between sites of FlAsH labeling (bottom) in the A-domain (i.e., interdomain spatial separation) or N-domain (intradomain spatial separation) relative to the nucleotide binding pocket in the N-domain (i.e., NH_1 side chain of Arg^{560} that functions to coordinate binding of the α-phosphoryl group of ATP (*13*)), using high-resolution structures of the Ca-ATPase stabilized in different enzymatic states (○) in comparison to experimental measurements using TNP-ATP as a FRET acceptor (●), normalized to an arbitrary reference point.

phosphoenzyme formation and calcium occlusion is facilitated upon occupancy of both high-affinity calcium binding sites (*41*).

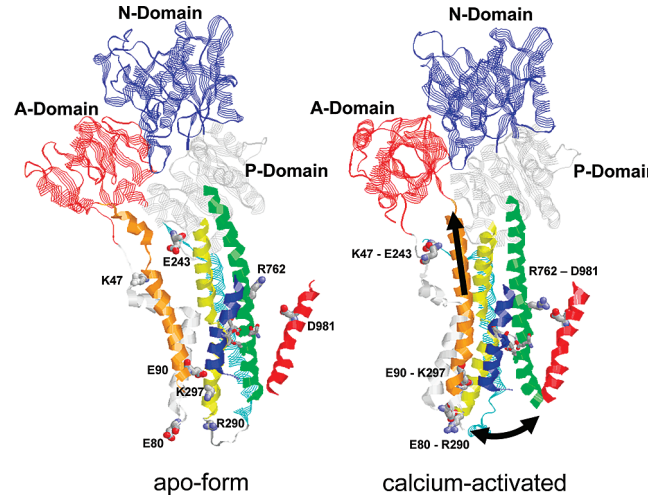

FIGURE 8: Calcium occupancy and concerted structural changes in transmembrane and cytosolic headpiece associated with occupancy of calcium binding site one and enzyme activation. Amino acids involved in calcium-dependent salt-bridges are highlighted in apo- (2c88.pdb) and calcium-activated (1t5s.pdb) forms of the Ca-ATPase. Arrows in 1t5s.pdb for the calcium-activated form highlight major calcium-dependent structural changes. Side chains associated with calcium binding to site one [involving ligands Asn^{768} and Glu^{771} in TM5 (green helix), Thr^{799} and Asp^{800} in TM6 (blue helix), and Glu^{908} in TM8 (not shown)] induce TM5 helix reorientation, bringing Arg^{762} (TM5) into the proximity of Asp^{981} (TM10 helix in red)) to form a stable salt bridge. Binding of the first calcium induces the formation of calcium binding site two (which shares calcium binding site Asn^{796} and Asp^{800} on TM6) with concomitant reorientation of TM4 to stabilize salt bridges (i) Glu^{80} (TM1/TM2 loop) with Arg^{290} (TM3/TM4 loop) and (ii) Glu^{90} in TM2 (orange helix) with Lys^{297} in TM4 (yellow helix) to form a helix bundle with the associated formation of the salt bridge between Lys^{47} and Glu^{243} located near the bilayer surface proximal to TM1 (white helix) and TM3 (cyan helix).

High-resolution structures indicate that Arg^{762} in TM5 can act as a molecular switch, since this residue has the potential to induce concerted movements of the transmembrane helices that facilitate the formation of high-affinity calcium binding sites and drive movements involving the cytosolic domain elements. Prior to calcium binding, Arg^{762} is proximal to both Asn^{768} (TM5) and Glu^{908} (TM8) within the bilayer interior. Upon calcium binding to site I, which includes ligands Asn^{768} and Glu^{908}, Arg^{762} is reoriented by a large-scale rotational movement of TM5 to create a new salt bridge with Asp^{981} on TM10 (Figure 8). Thus, charged side chains within the hydrophobic bilayer remain neutralized. The movement of TM5 and the creation of calcium binding site II promotes the formation of three additional salt bridges located near

the aqueous−bilayer interface, which would appear to stabilize the calcium-activated (E1) structure of the enzyme. These salt bridges include $Glu^{80}-Arg^{290}$ and $Glu^{90}-Lys^{297}$, which are respectively located in the loop structures of the lumenal interfacial regions connecting TM2/TM3 and TM4/TM5, and $Glu^{243}-Lys^{47}$ located at the cytoplasmic face of TM3 and TM1 (Figure 8).

Ligand binding of the second calcium involves Glu^{309} in TM4, whose conformational rearrangements can directly modify the position of the Asp^{351} side chain in the P-domain to facilitate the transfer of the γ-phosphoryl group of ATP bound to the N-domain to form the phosphoenzyme intermediate. The importance of site II occupancy in facilitating phosphoenzyme formation is apparent from (i) the calcium-dependent cooperativity associated with ATP hydrolysis that mirrors that associated with calcium binding (Figure 2) and (ii) a consideration of the plasma membrane Ca-ATPase (i.e., PMCA), which shares considerable structural homology with SERCA. In particular, a consideration of the sequence of the PMCA indicates a single high-affinity calcium binding site that is homologous to site II in SERCA (*42*). Moreover, the presence of only one high-affinity calcium site is consistent with the larger thermodynamic barrier opposing cation transport across the plasma membrane as compared with that of the sarcoplasmic reticulum. Thus, the calcium-dependent structural transitions and associated rearrangements of TM4 are conformationally coupled to the cytosolic headpiece elements to induce phosphoenzyme formation (*43*−*45*).

In conclusion, molecular probes bound specifically to engineered sites on the A- or N-domains of the Ca-ATP reveal coordinated but noncooperative domain movements associated with calcium activation. Large movements of the A-domain are observed, where the average structures of the physiologically important nucleotide bound states are in reasonable agreement with high-resolution crystal structures. Future measurements should measure the kinetics and magnitude of domain motions associated with enzyme activation, and the involvement of specific interfacial sites that stabilize the two major conformers (E1 and E2), taking advantage of the current ability to engineer multiple tags that bind unique small molecule probes (*18, 46*).

SUPPORTING INFORMATION AVAILABLE

Space-filling depictions of known structures of the Ca-ATPase in different enzyme states highlighting solvent accessibilities of proteinase K cleavage sites Leu^{119} and Thr^{242}. This material is available free of charge via the Internet at http://pubs.acs.org.

REFERENCES

1. Kuhlbrandt, W. (2004) Biology, structure and mechanism of P-type ATPases. *Nat. Rev. Mol. Cell Biol. 5*, 282–295.
2. Moller, J. V., Olesen, C., Jensen, A. M., and Nissen, P. (2005) The structural basis for coupling of Ca2+ transport to ATP hydrolysis by the sarcoplasmic reticulum Ca2+-ATPase. *J. Bioenerg. Biomembr. 37*, 359–364.
3. Olesen, C., Picard, M., Winther, A. M., Gyrup, C., Morth, J. P., Oxvig, C., Moller, J. V., and Nissen, P. (2007) The structural basis of calcium transport by the calcium pump. *Nature 450*, 1036–1042.
4. Toyoshima, C. (2008) Structural aspects of ion pumping by Ca(2+)-ATPase of sarcoplasmic reticulum. *Arch. Biochem. Biophys. 476*, 3–11.
5. Toyoshima, C., and Inesi, G. (2004) Structural basis of ion pumping by Ca2+-ATPase of the sarcoplasmic reticulum. *Annu. Rev. Biochem. 73*, 269–292.
6. Bigelow, D. J., and Inesi, G. (1992) Contributions of chemical derivatization and spectroscopic studies to the characterization of the Ca2+ transport ATPase of sarcoplasmic reticulum. *Biochim. Biophys. Acta 1113*, 323–338.
7. Sorensen, T. L., Moller, J. V., and Nissen, P. (2004) Phosphoryl transfer and calcium ion occlusion in the calcium pump. *Science 304*, 1672–1675.
8. Toyoshima, C., and Mizutani, T. (2004) Crystal structure of the calcium pump with a bound ATP analogue. *Nature 430*, 529–535.
9. Huang, S., and Squier, T. C. (1998) Enhanced rotational dynamics of the phosphorylation domain of the Ca-ATPase upon calcium activation. *Biochemistry 37*, 18064–18073.
10. Chen, B., Squier, T. C., and Bigelow, D. J. (2004) Calcium activation of the Ca-ATPase enhances conformational heterogeneity between nucleotide binding and phosphorylation domains. *Biochemistry 43*, 4366–4374.
11. Mueller, B., Zhao, M., Negrashov, I. V., Bennett, R., and Thomas, D. D. (2004) SERCA structural dynamics induced by ATP and calcium. *Biochemistry 43*, 12846–12854.
12. Inesi, G., Lewis, D., Ma, H., Prasad, A., and Toyoshima, C. (2006) Concerted conformational effects of Ca2+ and ATP are required for activation of sequential reactions in the Ca2+ ATPase (SERCA) catalytic cycle. *Biochemistry 45*, 13769–13778.
13. Ma, H., Inesi, G., and Toyoshima, C. (2003) Substrate-induced conformational fit and headpiece closure in the Ca2+ATPase (SERCA). *J. Biol. Chem. 278*, 28938–28943.
14. Squier, T. C., Bigelow, D. J., and Thomas, D. D. (1988) Lipid fluidity directly modulates the overall protein rotational mobility of the Ca-ATPase in sarcoplasmic reticulum. *J. Biol. Chem. 263*, 9178–9186.
15. Winters, D. L., Autry, J. M., Svensson, B., and Thomas, D. D. (2008) Interdomain fluorescence resonance energy transfer in SERCA probed by cyan-fluorescent protein fused to the actuator domain. *Biochemistry 47*, 4246–4256.
16. Picard, M., Toyoshima, C., and Champeil, P. (2005) The average conformation at micromolar [Ca2+] of Ca2+-atpase with bound nucleotide differs from that adopted with the transition state analog ADP.AlFx or with AMPPCP under crystallization conditions at millimolar [Ca2+]. *J. Biol. Chem. 280*, 18745–18754.
17. Inesi, G. (1985) Mechanism of calcium transport. *Annu. Rev. Physiol. 47*, 573–601.
18. Chen, B., Cao, H., Yan, P., Mayer, M. U., and Squier, T. C. (2007) Identification of an orthogonal peptide binding motif for biarsenical multiuse affinity probes. *Bioconjugate Chem. 18*, 1259–1265.
19. Menick, D. R., Lee, J. A., Brooker, R. J., Wilson, T. H., and Kaback, H. R. (1987) Role of cysteine residues in the lac permease of *Escherichia coli*. *Biochemistry 26*, 1132–1136.
20. van Iwaarden, P. R., Driessen, A. J., Menick, D. R., Kaback, H. R., and Konings, W. N. (1991) Characterization of purified, reconstituted site-directed cysteine mutants of the lactose permease of *Escherichia coli*. *J. Biol. Chem. 266*, 15688–15692.
21. van Iwaarden, P. R., Pastore, J. C., Konings, W. N., and Kaback, H. R. (1991) Construction of a functional lactose permease devoid of cysteine residues. *Biochemistry 30*, 9595–9600.
22. Jensen, A. M., Sorensen, T. L., Olesen, C., Moller, J. V., and Nissen, P. (2006) Modulatory and catalytic modes of ATP binding by the calcium pump. *EMBO J. 25*, 2305–2314.
23. Adams, S. R., Campbell, R. E., Gross, L. A., Martin, B. R., Walkup, G. K., Yao, Y., Llopis, J., and Tsien, R. Y. (2002) New biarsenical ligands and tetracysteine motifs for protein labeling in vitro and in vivo: Synthesis and biological applications. *J. Am. Chem. Soc. 124*, 6063–6076.
24. Griffin, B. A., Adams, S. R., and Tsien, R. Y. (1998) Specific covalent labeling of recombinant protein molecules inside live cells. *Science 281*, 269–272.
25. Waggoner, J. R., Huffman, J., Griffith, B. N., Jones, L. R., and Mahaney, J. E. (2004) Improved expression and characterization of Ca2+-ATPase and phospholamban in High-Five cells. *Protein Expression Purif. 34*, 56–67.
26. Lowry, O. H., Rosebrough, N. J., Farr, A. L., and Randall, R. J. (1951) Protein measurement with the Folin phenol reagent. *J. Biol. Chem. 193*, 265–275.
27. Lakowicz, J. (1999) *Principles of Fluorescence Specroscopy*, 2nd ed., Kluwer Academic/Plenum Publishers, New York.
28. Mahaney, J. E., Autry, J. M., and Jones, L. R. (2000) Kinetics studies of the cardiac Ca-ATPase expressed in Sf21 cells: new

insights on Ca-ATPase regulation by phospholamban. *Biophys. J. 78*, 1306–1323.

29. Verma, S., Xiong, Y., Mayer, M. U., and Squier, T. C. (2007) Remodeling of the bacterial RNA polymerase supramolecular complex in response to environmental conditions. *Biochemistry 46*, 3023–3035.
30. Luedtke, N. W., Dexter, R. J., Fried, D. B., and Schepartz, A. (2007) Surveying polypeptide and protein domain conformation and association with FlAsH and ReAsH. *Nat. Chem. Biol. 3*, 779–784.
31. Chen, B., Mayer, M. U., Markillie, L. M., Stenoien, D. L., and Squier, T. C. (2005) Dynamic motion of helix A in the amino-terminal domain of calmodulin is stabilized upon calcium activation. *Biochemistry 44*, 905–914.
32. Chen, B., Mayer, M. U., and Squier, T. C. (2005) Structural uncoupling between opposing domains of oxidized calmodulin underlies the enhanced binding affinity and inhibition of the plasma membrane Ca-ATPase. *Biochemistry 44*, 4737–4747.
33. Giepmans, B. N., Adams, S. R., Ellisman, M. H., and Tsien, R. Y. (2006) The fluorescent toolbox for assessing protein location and function. *Science 312*, 217–224.
34. Toyoshima, C., Nakasako, M., Nomura, H., and Ogawa, H. (2000) Crystal structure of the calcium pump of sarcoplasmic reticulum at 2.6 Å resolution. *Nature 405*, 647–655.
35. Toyoshima, C., and Nomura, H. (2002) Structural changes in the calcium pump accompanying the dissociation of calcium. *Nature 418*, 605–611.
36. Watanabe, T., and Inesi, G. (1982) The use of 2′,3′-O-(2,4,6-trinitrophenyl) adenosine 5′-triphosphate for studies of nucleotide interaction with sarcoplasmic reticulum vesicles. *J. Biol. Chem. 257*, 11510–11516.
37. Nakamoto, R. K., and Inesi, G. (1984) Studies of the interactions of 2′,3′-O-(2,4,6-trinitrocyclohexyldienylidine)adenosine nucleotides with the sarcoplasmic reticulum (Ca2+ + Mg2+)-ATPase active site. *J. Biol. Chem. 259*, 2961–2970.
38. Hua, S., Ma, H., Lewis, D., Inesi, G., and Toyoshima, C. (2002) Functional role of "N" (nucleotide) and "P" (phosphorylation) domain interactions in the sarcoplasmic reticulum (SERCA) ATPase. *Biochemistry 41*, 2264–2272.
39. Bigelow, D. J., Squier, T. C., and Thomas, D. D. (1986) Temperature dependence of rotational dynamics of protein and lipid in sarcoplasmic reticulum membranes. *Biochemistry 25*, 194–202.
40. Inesi, G., Kurzmack, M., Coan, C., and Lewis, D. E. (1980) Cooperative calcium binding and ATPase activation in sarcoplasmic reticulum vesicles. *J. Biol. Chem. 255*, 3025–3031.
41. Inesi, G., and de Meis, L. (1989) Regulation of steady state filling in sarcoplasmic reticulum. Roles of back-inhibition, leakage, and slippage of the calcium pump. *J. Biol. Chem. 264*, 5929–5936.
42. Di Leva, F., Domi, T., Fedrizzi, L., Lim, D., and Carafoli, E. (2008) The plasma membrane Ca(2+) ATPase of animal cells: Structure, function and regulation. *Arch. Biochem. Biophys. 476*, 65–74.
43. Clarke, D. M., Loo, T. W., Rice, W. J., ersen, J. P., Vilsen, B., and MacLennan, D. H. (1993) Functional consequences of alterations to hydrophobic amino acids located in the M4 transmembrane sector of the Ca(2+)-ATPase of sarcoplasmic reticulum. *J. Biol. Chem. 268*, 18359–18364.
44. Rice, W. J., Green, N. M., and MacLennan, D. H. (1997) Site-directed disulfide mapping of helices M4 and M6 in the Ca2+ binding domain of SERCA1a, the Ca2+ ATPase of fast twitch skeletal muscle sarcoplasmic reticulum. *J. Biol. Chem. 272*, 31412–31419.
45. Skerjanc, I. S., Toyofuku, T., Richardson, C., and MacLennan, D. H. (1993) Mutation of glutamate 309 to glutamine alters one Ca(2+)-binding site in the Ca(2+)-ATPase of sarcoplasmic reticulum expressed in Sf9 cells. *J. Biol. Chem. 268*, 15944–15950.
46. Cao, H., Xiong, Y., Wang, T., Chen, B., Squier, T. C., and Mayer, M. U. (2007) A red cy3-based biarsenical fluorescent probe targeted to a complementary binding peptide. *J. Am. Chem. Soc. 129*, 8672–8673.
47. Ma, H., Lewis, D., Xu, C., Inesi, G., and Toyoshima, C. (2005) Functional and structural roles of critical amino acids within the"N", "P", and "A" domains of the Ca2+ ATPase (SERCA) headpiece. *Biochemistry 44*, 8090–8100.
48. Toyoshima, C., Nomura, H., and Tsuda, T. (2004) Lumenal gating mechanism revealed in calcium pump crystal structures with phosphate analogues. *Nature 432*, 361–368.
49. Olesen, C., Sorensen, T. L., Nielsen, R. C., Moller, J. V., and Nissen, P. (2004) Dephosphorylation of the calcium pump coupled to counterion occlusion. *Science 306*, 2251–2255.

BI8014289